Arch. Metall. Mater. **66** (2021), 4, 1013-1018

DOI: 10.24425/amm.2021.136416

SEUNG Y. YANG[1,2], BONG H. KIM[1*], DA B. LEE[1], KWEON H. CHOI[1], NAM S. KIM[1], SEONG H. HA[1], YOUNG O. YOON[1], HYUN K. LIM[1], SHAE KIM[1], YOUNG J. KIM[2]

WARM TENSILE DEFORMATION BEHAVIOR AND CONSTITUTIVE EQUATION OF SUPERSATURATED SOLID-SOLUTIONIZED Al-9Mg EXTRUDED ALLOY

In this paper, as a purpose to apply the supersaturated solid-solutionized Al-9Mg alloy to the structural sheet parts of automotive, tensile tests were conducted under the various conditions and a constitutive equation was derived from the tensile test results. Al-9Mg alloy was produced using a special Mg master alloy containing Al_2Ca during the casting process and extruded into the sheet. In order to study the deformation behavior of Al-9Mg alloy in warm temperature forming environments, tensile tests were conducted under the temperature of 373 K-573 K and the strain rate of 0.001/s~0.1/s. In addition, by using the raw data obtained from tensile tests, a constitutive equation of the Al-9Mg alloy was derived for predicting the optimized condition of the hot stamping process. Al-9Mg alloy showed uncommon deformation behavior at the 373 K and 473 K temperature conditions. The calculated curves from the constitutive equation well-matched with the measured curves from the experiments particularly under the low temperature and high strain rate conditions.

Keywords: Aluminum alloy, Al-9Mg alloy, Tensile test, Constitutive equation

1. Introduction

Strict environmental regulations and the growth of the electric vehicle market have made aluminum alloys more attractive in the automotive industry. Among aluminum alloys, 5xxx series aluminum alloys have been used primarily in the automotive inner panel due to their good mechanical property, weldability, corrosion resistance, and formability [1]. Solid-solution strengthening is one of the main strengthening mechanisms of 5xxx series aluminum alloys due to Mg solute atoms. So, the strength of 5xxx series aluminum alloys improves as Mg content increases. In addition, an increase in the Mg content lowers the Stacking Fault Energy (SFE) of 5xxx series aluminum alloys, increasing strength and elongation simultaneously [2]. But the strong oxidation tendency of Mg has limited the Mg contents of commercial alloys to less than 5%. However, it was recently reported that the usage of Mg master alloy including Al_2Ca in the alloying process significantly inhibits the oxidation of Mg. This technology makes it possible to produce Al-xMg ($x \geq 5\%$) alloys having excellent mechanical properties without loss of quality.

It is generally known that sheet forming of the aluminum alloys at room temperature is difficult owing to poor plasticity and severe springback phenomenon [1,3]. For this reason, the forming process of the aluminum alloys sheet has been conducted at elevated temperature conditions. Therefore, to predict the sheet formability, it is necessary to study the deformation behavior of 5xxx series aluminum alloys under warm forming conditions.

Warm deformation behavior of Al-xMg ($x \geq 5\%$) alloys with better mechanical properties than commercial 5xxx series alloys has been studied, but most of the literature has analyzed the deformation behavior in compressive mode [4]. In terms of sheet forming, however, deformation behavior in the tensile mode has a more important meaning. The flow stress curves in the compressive mode are measured up to around 1.0 of the true strain under all test conditions, except for infrequent failures during test. So, the difference in the degree of deformation to fracture for each sheet forming condition cannot be compared from the flow stress curves in the compressive mode. On the other hand, the flow stress curves in the tensile mode show different strain to fracture for each forming condition. Besides, the strain hardening index (n) and the strain rate sensitivity exponent (m),

[1] KOREA INSTITUTE OF INDUSTRIAL TECHNOLOGY, ADVANCED PROCESS AND MATERIALS R&D GROUP, KITECH, 156 GAETBEOL RD., YEONSU-GU, INCHEON, 21999, KOREA
[2] SUNGKYUNKWAN UNIVERSITY, ADVANCED MATERIALS SCIENCE & ENGINEERING, SKKU, SUWON, KOREA

* Corresponding author: bonghk75@kitech.re.kr

which are known to have a critical effect on sheet formability, can be derived from the tensile test result data [5,6]. Therefore, many works of literature carried out tensile tests for predicting sheet formability.

In this paper, supersaturated solid-solutionized Al-9Mg alloy was tensile tested under various warm deformation conditions for understanding the deformation behavior of Al-9Mg alloy at elevated temperatures. Tensile tests were carried out under the temperature range of 373-573 K and the strain rate range of 0.001-0.1 /s. Additionally, to predict optimized hot stamping conditions, a constitutive equation considering temperature and strain rate as variables was derived from tensile test results. Calculated curves from the constitutive equation were compared with measured curves obtained from the experiments.

2. Experimental

Extruded Al-9Mg alloy sheet was studied in this paper. Table 1 shows the chemical composition of the Al-9Mg alloy. The billet of the Al-9Mg alloy with a diameter of 7 inches was produced using Mg master alloy including Al_2Ca through the Direct Chill casting process. Homogenization heat treatment was conducted at 693 K for 24 h. The homogenized billet was extruded to sheets with a width of 100 mm and a thickness of 12 mm using a direct extruder. The extrusion ratio was 20.7:1 and ram speed was about 0.5 mm/s. For the tensile test, Al-9Mg alloy sheets were machined to the specimen with a gauge length of 8 mm, a width of 3 mm, and a thickness of 3 mm along the extrusion direction as shown in Fig. 1. Tensile tests were carried out under the temperature conditions of 373 K, 473 K, and 573 K and the strain rate conditions of 0.001 /s, 0.01 /s, and 0.1 /s. Before the tests, the specimen was preheated in the furnace attached to the tensile test machine at the test temperature for 20 minutes. For observing grain size and shape in the TD plane, the tested specimen was polished and electrolytic etched with Barker's reagent. The raw data of tensile test results were processed to true stress and strain data for calculating the constitutive equation of the Al-9Mg sheet. The constitutive equation was derived based on the Fields-Backofen equation. Fields-Backofen equation is one of the equations which can express the flow stress curve of materials considering the strain hardening effect. Also, it has the advantage of taking temperature and strain rate into account. This equation is structured as follows:

$$\sigma = K\varepsilon^n \dot{\varepsilon}^m \quad (1)$$

where, σ is the true stress, K is the strength coefficient, ε is the true strain, n is the strain hardening index, $\dot{\varepsilon}$ is the strain rate, and m is the strain rate sensitivity exponent.

TABLE 1

The chemical composition of the Al-9Mg alloy

Alloy	Si	Fe	Mg	Ti	Ca	Al
Al-9Mg	0.02	0.08	8.85	0.03	0.06	Balance

3. Results and discussion

The engineering stress-strain curves of the Al-9Mg alloy under various test conditions are shown in Fig. 2 (a), (b), and (c). In addition, Fig. 2 (d), (e), and (f) display the true stress-strain curves calculated from the engineering stress-strain curves. Under the low temperature and high strain rate conditions, strain hardening region prominently appeared after elastic region. This is because the multiplication of dislocations predominated over the annihilation of dislocations. On the other hand, under the high temperature and low strain rate conditions, softening region occurred following the peak stress point, indicating that the annihilation of dislocations was dominant and dynamic restoration operated. Under the 373 K conditions, however, it is noted that the stress was highest at the strain rate of 0.01/s as shown in Fig. 3. This is due to Dynamic Strain Aging (DSA) phenomenon. The Mg solute atoms strongly interact with dislocations and interrupt the movement of them. Dislocations that escape from the interference of Mg atoms by higher stress are again disturbed by Mg atoms due to the high mobility of Mg atoms in the Al matrix. Therefore, DSA mainly appears under certain deformation conditions, where the Mg atoms move faster than dislocations and lock again the moving dislocations. For this reason, under the 373 K conditions, the highest peak stress appeared at the medium strain rate condition, unlike the general deformation behavior. When DSA appears, the strain rate sensitivity exponent has a negative value [7,8]. Therefore,

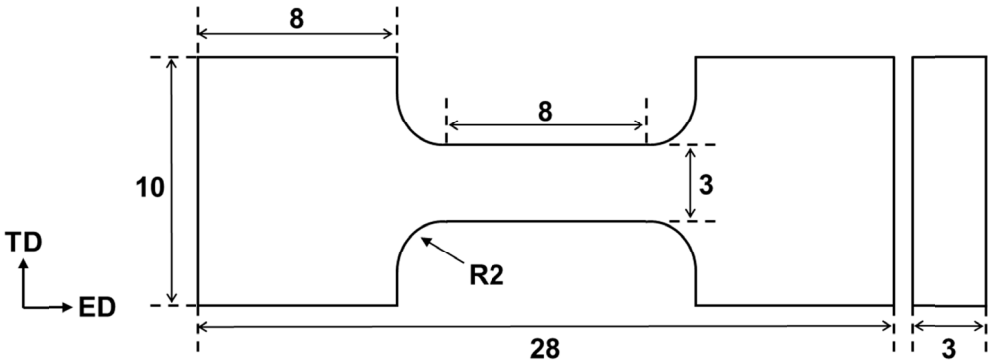

Fig. 1. Geometry of the tensile test specimen (length unit: mm) (TD = Transverse Direction, ED = Extrusion Direction)

this is also called Negative Strain Rate Sensitivity(n-SRS) phenomenon. On the other hand, under the 473 K conditions, the true strain showed rather a decrease as the strain rate decreased. This uncommon tendency is assumed to appear due to the defects occurring during the warm deformation at the grain boundaries. Fig. 4 (a), (b), and (c) show the etched microstructure images of specimens tested at the 474 K conditions observed with a polarizing filter. It can be seen that the microstructure of the three specimens consisted of similar grains in shape and size. Fig. 4 (c), (d), and (e) display the etched microstructure images at the 474 K conditions observed without a polarizing filter. It is noted that there were only cavities arranged along the extrusion direction under the 0.1 /s condition. However, the cavities that distributed at the grain boundaries were also observed under the 0.01 /s and 0.001 /s conditions. Moreover, the microstructure of the 0.001 /s condition had more cavities than the microstructure of the 0.01 /s condition. The occurrence of cavities at the grain boundaries is due to the second-phase particles precipitated on the grain boundaries and the operation of grain boundary sliding. The Al-9Mg alloy has a large amount of second-phase particles

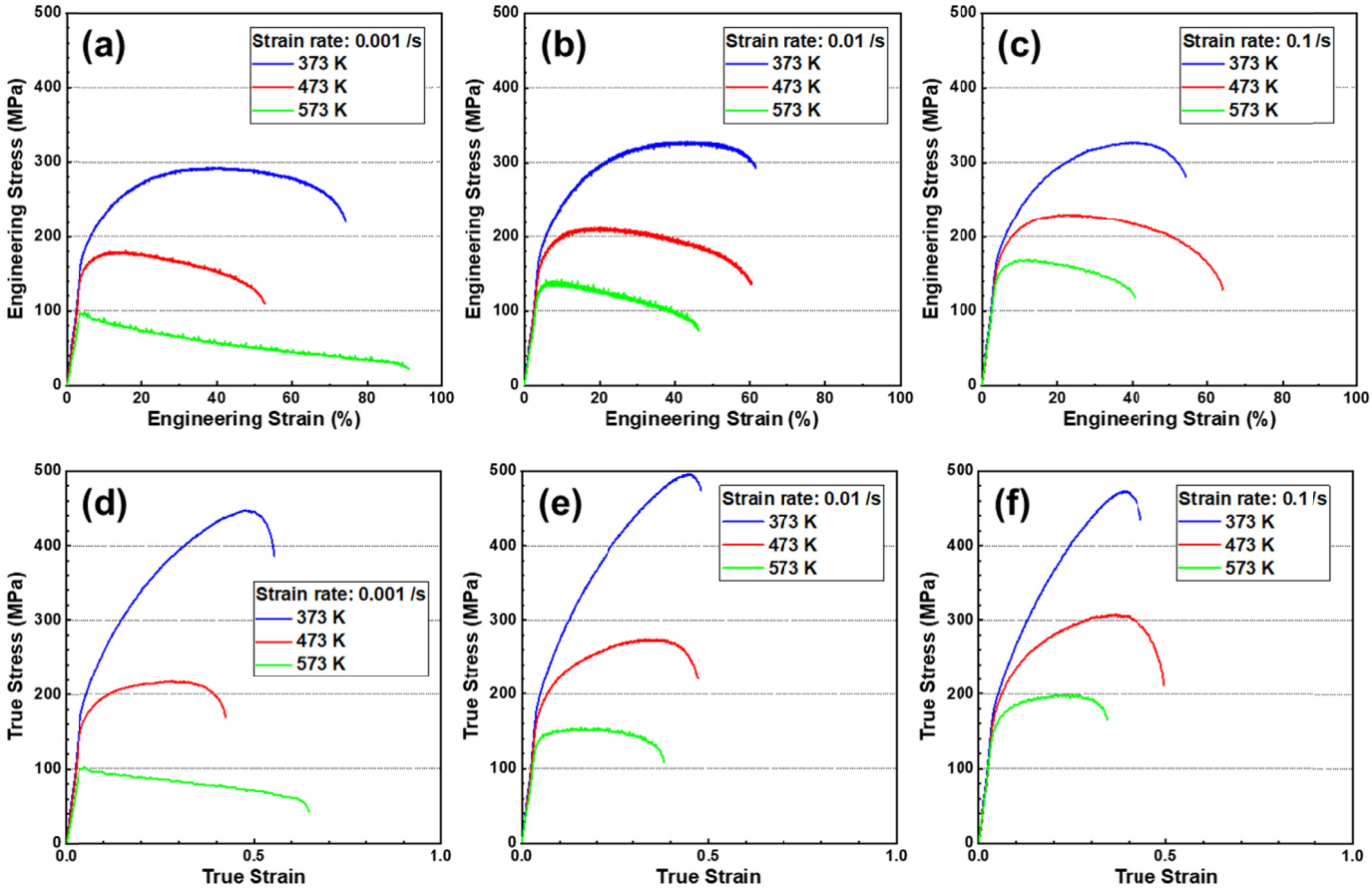

Fig. 2. Engineering stress-strain curves of the Al-9Mg at the temperature of 373-573 K and the strain rate of (a) 0.001 /s, (b) 0.01 /s, and (c) 0.1 /s and true stress-strain curves at the temperature of 373-573 K and the strain rate of (d) 0.001 /s, (e) 0.01 /s, and (f) 0.1 /s

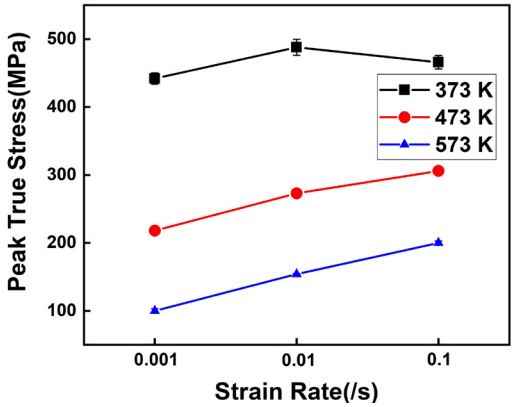

Fig. 3. Peak true stress of 373-573 K temperature conditions as a function of the strain rate

owing to its high Mg content, and the particles preferentially precipitate on the grain boundaries that have high energy. These particles act as a site for the generation of cavities during the deformation. Besides, under the conditions of high temperature and low strain rate, the grain boundary sliding, one of the deformation mechanisms, operates and develops the cavities at the grain boundaries. The cavities generated for these reasons have an adverse effect on the mechanical properties [9]. Therefore, contrary to the general tendency, the low strain rate condition showed a lower true strain than the high strain rate condition.

From the true stress-strain curves presented in Fig. 2 (d), (e), and (f), a constitutive equation that can express the warm tensile deformation behavior of Al-9Mg alloy was derived. The three factors constituting the Fields-Backofen equation, the strain

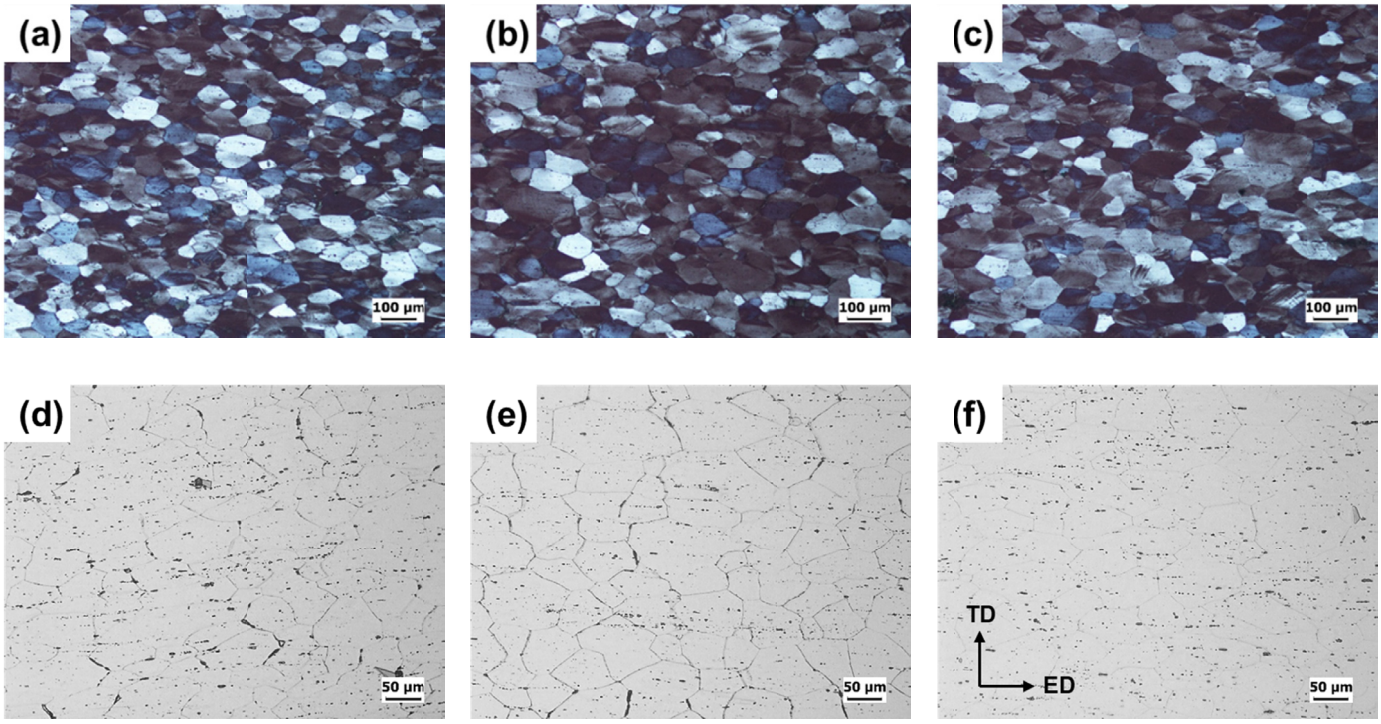

Fig. 4. The etched microstructure images of tested specimens under the 473 K and (a) 0.001 /s, (b) 0.01 /s, and (c) 0.1 /s observed with a polarizing filter, and the images of tested specimens under the 473 K and (d) 0.001 /s, (e) 0.01 /s, and (f) 0.1 /s observed without a polarizing filter

hardening index (n), the strain rate sensitivity exponent (m), and the strength coefficient (K) were obtained as follows. The strain hardening index (n), which shows the ability to deform uniformly before necking [10,11], can be expressed as the following equation from the Fields-Backofen equation.

$$n = \left.\frac{d\log\sigma}{d\log\varepsilon}\right|_{\dot{\varepsilon},T} \tag{2}$$

Fig. 5 displays a linear relationship between n obtained from Eq. (2) and the reciprocal of temperature and logarithmic strain rate. From this relationship, n can be expressed as follows [12-14].

$$n = A\log\dot{\varepsilon} + B/T(K) + C \tag{3}$$

Parameter A, B, and C can be calculated from the slope and y-intercept of the lines through the equalization treatment [13]. So, n of Al-9Mg alloy can be described as Eq. (4).

$$n = -0.59299 + 0.05929\cdot\log\dot{\varepsilon} + 428.21287/T \tag{4}$$

The strain rate sensitivity exponent (m), which means how much the material can resist necking [14], can be obtained in the form of Eq. (5) according to Eq. (1),

$$m = \left.\frac{d\log\sigma}{d\log\dot{\varepsilon}}\right|_{\varepsilon,T} \tag{5}$$

Fig. 6 (a) shows $\log\sigma$ – $\log\dot{\varepsilon}$ plots at ε = 0.1, 0.14, and 0.18. From Eq. (5), it can be seen that m is the slope of each

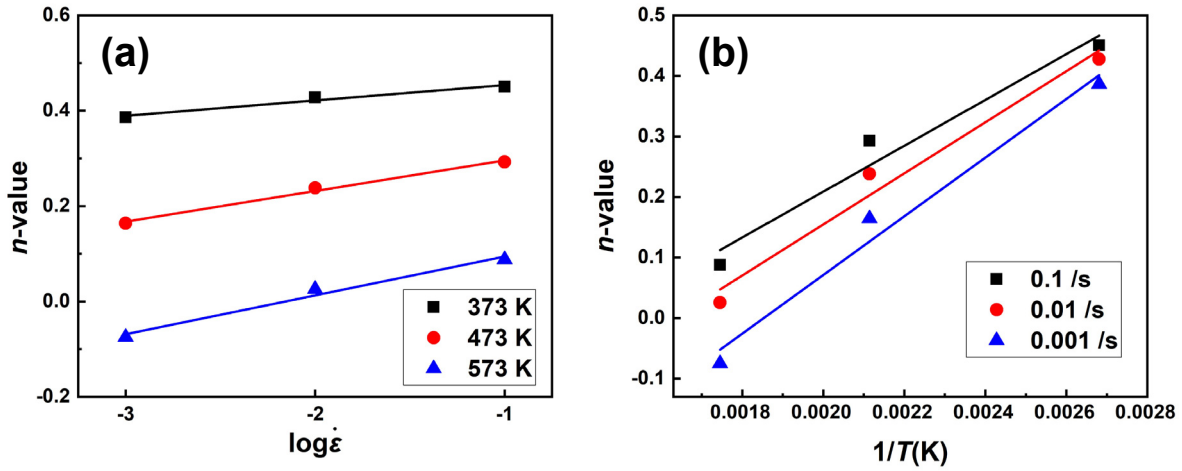

Fig. 5. Relationship between n-value and (a) logarithmic strain rate and (b) reciprocal of temperature

temperature condition graph. m was plotted as a function of the temperature in Fig. 6(b). Through polynomial fitting, m of Al-9Mg alloy can be established as Eq. (6).

$$m = 0.52115 - 0.00279 \cdot T + 3.6695 \cdot 10^{-6} \cdot T^2 \quad (6)$$

The strength coefficient (K) calculated from Eq. (1) was plotted as a function of the reciprocal of temperature and logarithmic strain rate in Fig. 7. From Fig. 7, it can be seen that K also had a linear relationship with the reciprocal of temperature and logarithmic strain rate as n. Therefore, K can be obtained in the same way as n as follows.

$$K = -467.20527 + 57.99926 \cdot \log \dot{\varepsilon} + 5.00383 \cdot 10^5 / T \quad (7)$$

Fig. 8 shows the measured curves from the tests and the calculated curves obtained from the factors derived above. It can be seen that the calculated curves agreed well with the measured

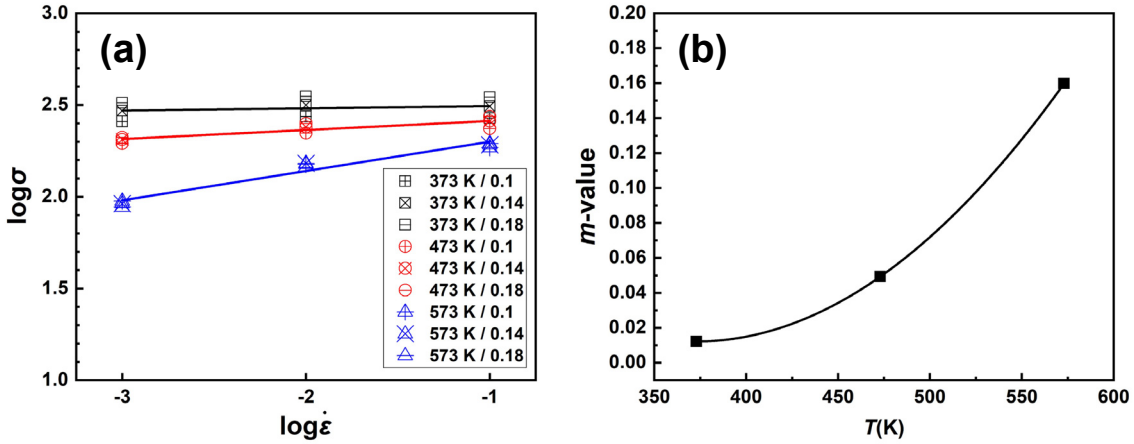

Fig. 6. (a) Relationship between logarithmic true stress and logarithmic strain rate and (b) Relationship between m-value and test temperatures

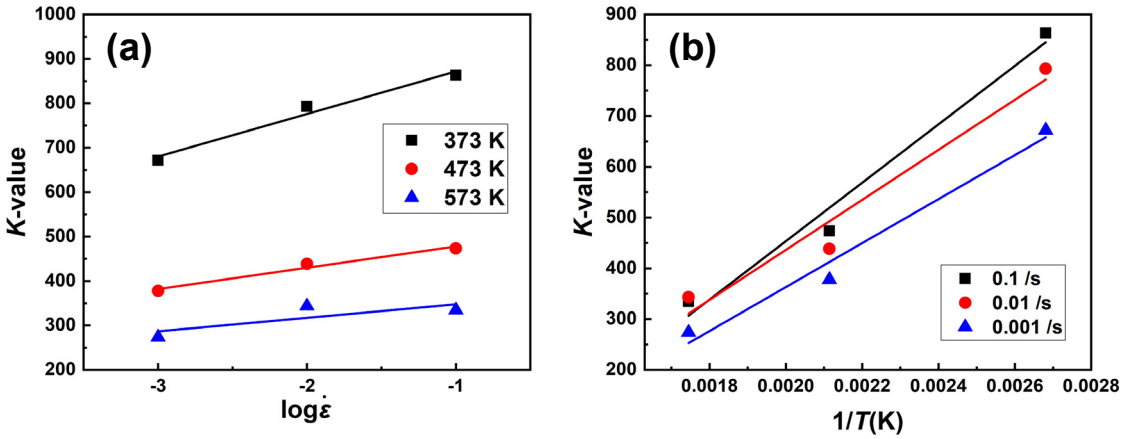

Fig. 7. Relationship between K-value and (a) logarithmic strain rate and (b) reciprocal of temperature

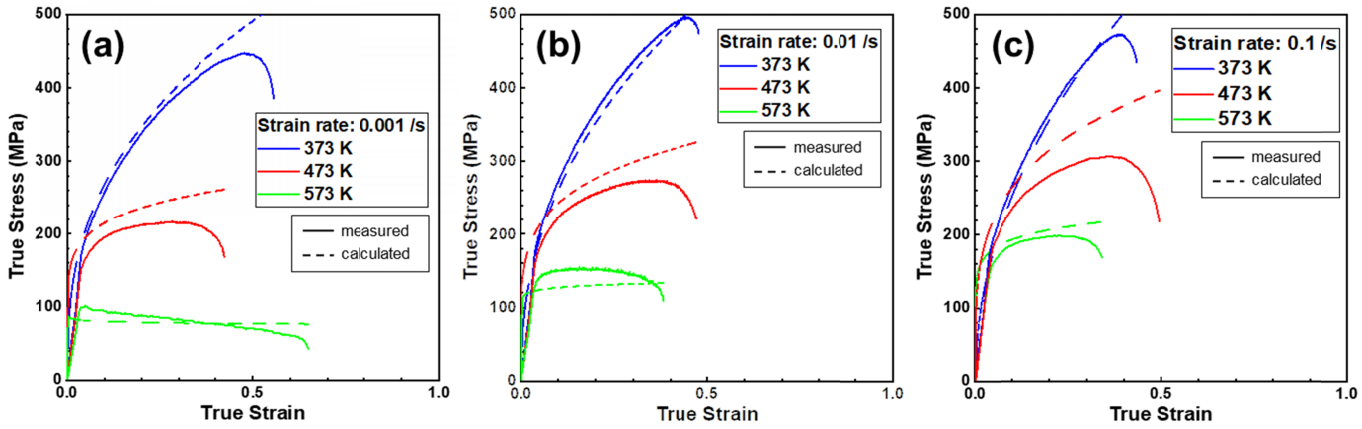

Fig. 8. Comparison between the calculated curves and the measured curves under (a) 0.001 /s, (b) 0.01 /s, and (c) 0.1 /s conditions

curves under the conditions of low temperature and high strain rate. However, the Fields-Backofen equation can represent only the strain hardening region where the material is deformed by the glide of dislocations. Therefore, the softening region where the material is deformed by the climb of dislocations cannot be predicted [15].

4. Conclusions

In this paper, the flow stress behavior of supersaturated solid-solutionized Al-9Mg alloy was studied through tensile test under the various temperature and strain rate conditions for applying this alloy to the automotive industry. Unlike previous research that analyzed the deformation behavior only in the compressive mode, this paper is the first to study the deformation behavior of Al-9Mg alloy in the tensile mode. And the constitutive equation was derived from the tensile test results to predict the optimized condition of the hot stamping process. Besides, the calculated curves and measured curves were compared to validate the accuracy of the constitutive equation. From the tensile test results, it was confirmed that the DSA phenomenon appears at 373 K condition in the Al-9Mg alloy. In addition, the ductility decreased as the strain rate decreased due to cavities at the grain boundaries. The constitutive equation of Al-9Mg alloy obtained using the tensile test results is as follows.

$$\begin{cases} \sigma = K\varepsilon^{n}\dot{\varepsilon}^{m} \\ n = -0.59299 + 0.05929\log\dot{\varepsilon} + 428.21287/T \\ m = 0.52115 - 0.00279\cdot T + 3.6695\cdot 10^{-6}\cdot T^{2} \\ K = -467.20527 + 57.99926\log\dot{\varepsilon} + 5.00383/T \end{cases} \quad (8)$$

The calculated curves by the constitutive equation matched well with the measured curves under the low temperature and high strain rate conditions, except for the softening region owing to the limitation of the Field-Backofen equation.

REFERENCES

[1] P.F. Bariani, S. Bruschi, A, Ghiotti, F. Michieletto, CIRP Annals **62**, 251-254 (2013). DOI: https://doi.org/10.1016/j.cirp.2013.03.050

[2] B.-H. Lee, S.-H. Kim, J.-H. Park, H.-W. Kim, J.-C. Lee, Materials Science and Engineering: A **657**, 115-122 (2016). DOI: https://doi.org/10.1016/j.msea.2016.01.089

[3] D. Li, A. Ghosh, Materials Science and Engineering: A **352**, 279-286 (2003). DOI: https://doi.org/10.1016/S0921-5093 (02)00915-2

[4] N.-S. Kim, K.-H. Choi, S.-Y. Yang, S.-H. Ha, Y.-O. Yoon, B.-H. Kim, H.-K. Lim, S.K. Kim, S.-K. Hyun, Metals **11**, 288 (2021). DOI: https://doi.org/10.3390/met11020288

[5] H. Wang, Y. Luo, P. Friedman, M. Chen, L. Gao, Transactions of Nonferrous Metals Society of China **22**, 1-7 (2012). DOI: https://doi.org/10.1016/S1003-6326(11)61131-X

[6] D. Li, A.K. Ghosh, Journal of Materials Processing Technology **145**, 281-293 (2004). DOI: https://doi.org/10.1016/j.jmatprotec.2003.07.003

[7] R.C. Picu, Acta Materialia **52**, 3447-3458 (2004). DOI: https://doi.org/10.1016/j.actamat.2004.03.042

[8] C.-H. Cho, H.-W. Son, J.-C. Lee, K.-T. Son, J.-W. Lee, S.-K. Hyun, Materials Science and Engineering: A **779**, 139151 (2020). DOI: https://doi.org/10.1016/j.msea.2020.139151

[9] S.-Y. Yang, D.-B. Lee, K.-H. Choi, N.-S. Kim, S.-H. Ha, B.-H. Kim, Y.-O. Yoon, H.-K. Lim, S.K. Kim, Y.-J. Kim, Metals **11**, 410 (2021). DOI: https://doi.org/10.3390/met11030410

[10] Q. Dai, Y. Deng, H. Jiang, J. Tang, J. Chen, Materials Science and Engineering: A, **766**, 138325 (2019). DOI: https://doi.org/10.1016/j.msea.2019.138325

[11] L. Hua, F. Meng, Y. Song, J. Liu, X. Qin, L. Suo, J. of Materi Eng and Perform **23**, 1107-1113 (2014). DOI: https://doi.org/10.1007/s11665-013-0834-2

[12] Y.Q. Cheng, H. Zhang, Z.H. Chen, K.F. Xian, Journal of Materials Processing Technology **208**, 29-34 (2008). DOI: https://doi.org/10.1016/j.jmatprotec.2007.12.095

[13] L.C. Tsao, H.Y. Wu, J.C. Leong, C.J. Fang, Materials & Design **34**, 179-184 (2012). DOI: https://doi.org/10.1016/j.matdes.2011.07.060

[14] K.C. Chan, G.Q. Tong, Materials Letters **51**, 389-395 (2001).

[15] https://www.sentesoftware.co.uk/site-media/flow-stress-curve